Soil moisture–atmosphere coupling amplifies the change in extreme heat in inner East Asia under rapid summer warming

ENVIRONMENTAL RESEARCH
LETTERS

PURPOSE-LED PUBLISHING™

LETTER • OPEN ACCESS

Soil moisture–atmosphere coupling amplifies the change in extreme heat in inner East Asia under rapid summer warming

To cite this article: Zejiang Yin *et al* 2025 *Environ. Res. Lett.* **20** 014022

ENVIRONMENTAL RESEARCH
LETTERS

LETTER

Soil moisture–atmosphere coupling amplifies the change in extreme heat in inner East Asia under rapid summer warming

Zejiang Yin[1], Buwen Dong[2], Song Yang[1,3,*] and Wei Wei[1,3]

[1] School of Atmospheric Sciences, Sun Yat-sen University, and Southern Marine Science and Engineering Guangdong Laboratory (Zhuhai), Zhuhai, People's Republic of China
[2] National Centre for Atmospheric Science, Department of Meteorology, University of Reading, Reading, United Kingdom
[3] Guangdong Province Key Laboratory for Climate Change and Natural Disaster Studies, Sun Yat-sen University, Zhuhai, People's Republic of China
* Author to whom any correspondence should be addressed.

E-mail: yangsong3@mail.sysu.edu.cn

Keywords: extreme heat, climate change, trajectory, land-atmosphere feedback

Supplementary material for this article is available online

OPEN ACCESS

RECEIVED
1 September 2024

REVISED
7 October 2024

ACCEPTED FOR PUBLICATION
21 November 2024

PUBLISHED
13 December 2024

Abstract

Inner East Asia (IEA) is an important component of the global grassland ecosystem and has experienced a more rapid increase in extreme surface air temperatures compared to the summer mean in recent decades (2001–2020, relative to 1971–1990). This excess hot-extreme warming (EHEW) is particularly pronounced in the southern IEA, where extremely hot temperatures have increased twice as quickly as the summer mean warming, which itself already exceeds global-land warming by more than threefold. A quantitative analysis based on a Lagrangian temperature-anomaly equation along air-parcel backward trajectories initiated on hot days across IEA reveals that the observed EHEW is primarily attributable to increased diabatic heating, which predominantly occurs from 2 days before to the hot days. Meanwhile, changes in heat-prone synoptic-scale circulation only exert a limited influence on the excess warming. Soil drying within IEA appears to be a critical factor contributing to increased diabatic heating through soil moisture–atmosphere coupling, as it limits evaporation and enhances sensitive heat flux, thereby triggering positive soil moisture-temperature feedback. Our analysis underscores the significant impact of local soil moisture deficits on the intensified extreme heat. Urgent implementation of grassland and livestock management strategies, coupled with drought mitigation measures, is essential for adaptation and ecosystem conservation.

1. Introduction

Inner East Asia (IEA), including Mongolia and its surroundings (figure 1(b)), is a crucial part of the global grassland ecosystem and exerts vital influences on East Asian and global carbon cycles (Gang *et al* 2014). It has supported pastoralists for thousands of years and currently sustains approximately 70 million livestock, providing livelihoods for 29% of Mongolia's working-age population, contributing about 15% of the national GDP (Nandintsetseg *et al* 2021). However, these grassland ecosystems are fragile and particularly vulnerable to climate change and human activities due to their presence in arid and semi-arid climate regions (Na *et al* 2021, Zhao *et al* 2021). Since the early 2000s, IEA has experienced dramatic warming in the boreal summer, potentially reaching a tipping point and implying irreversible regional climate change (Dong *et al* 2016, Zhang *et al* 2020b, Cai *et al* 2024). Along with this rapid warming, extremely high temperatures have remarkably increased, often occurring concurrently with extreme dryness (Zhang *et al* 2020b, Seo and Ha 2022). This combination can have severe and complex impacts on biological systems, particularly affecting grasslands including decreased biomass, plant mortality, and potential shifts in ecosystems from carbon sinks to carbon sources (Easterling *et al* 2000, Chen *et al* 2023, Zhang *et al* 2024a). In fact, these climate changes, compounded by the effect of overgrazing, have led to widespread degradation of grasslands, environmental deterioration, and desert expansion

on IEA, threatening long-term livestock production and food security (Bouwman *et al* 2005, Hilker *et al* 2014, Zhang *et al* 2020c, Nandintsetseg *et al* 2021). Therefore, understanding the physical processes behind the abrupt increase in the extremely hot temperatures in this century is critical to mitigating ecological and social risks.

IEA summer warming could shift the daily air temperature distribution toward higher values, resulting in increased hot-extreme temperatures (Donat and Alexander 2012, Lewis and King 2017). This summer's warming is driven by both external forcing and internal climate variability. Specifically, increased anthropogenic greenhouse gas emissions and decreased anthropogenic aerosols explain more than half of the observed rapid warming (Dong *et al* 2016, Zhou *et al* 2020, Hua *et al* 2021, Zhang *et al* 2024b). Additionally, both observations and model simulations have demonstrated that the changes in the phase of two interdecadal sea surface temperature variabilities, the interdecadal pacific variability (IPV) and the Atlantic multidecadal variability (AMV), have decisively influenced the recent warming (Cai *et al* 2019, 2024, Zhang *et al* 2024b). These changes trigger or contribute to atmospheric Rossby wave trains across the northern mid-latitudes, thereby contributing to an anticyclonic circulation anomaly over IEA, which could intensify surface warming through adiabatic heating and increased surface solar radiation (Hong *et al* 2017, Piao *et al* 2017, Zhang *et al* 2020a, Sun *et al* 2022).

Furthermore, over the past two decades, hot extremes over IEA have exhibited excess warming rates compared to the summer mean temperatures (figure 1(d)), thereby exacerbating the ecosystem vulnerability to abrupt warming. This excess hot-extreme warming (EHEW) suggests alterations in the shape of the temperature distribution and underscores the physical mechanisms for the intensified extreme warming. Three physical processes have been identified as contributing to the hot extremes: temperature advection, adiabatic compression, and diabatic heating (Röthlisberger and Papritz 2023). The dynamic or thermodynamic drivers that enhance these physical processes can create conditions that amplify hot extremes. For instance, changes in atmospheric circulation that result in prolonged and intensified heat-prone weather regimes can exacerbate extreme warming (Mann *et al* 2017, Kornhuber *et al* 2019, Teng and Branstator 2019). Differential heating rates across latitudes may lead to nonlinear changes in temperature advection under various weather regimes, facilitating the transport of hot air in heat-prone circulation conditions and amplifying extreme warming (Tamarin-Brodsky *et al* 2022, Patterson 2023). Moreover, soil moisture conditions can exert a nonlinear control over energy partitioning between latent and sensible heats, thereby mitigating or amplifying extreme temperatures (Seneviratne *et al* 2006, 2010, Perkins *et al* 2015, Qiao *et al* 2023, Cai *et al* 2024, Zuo *et al* 2024). In wet energy-limited conditions where soil moisture allows for unrestricted evaporation, soil moisture depletion coincides with enhanced latent heat, which effectively restrains the increases in sensible heat flux and air temperature. Conversely, under water-limited conditions with drying soils, reduced soil moisture restricts evaporation and decreases latent heat, which in turn increases sensible heat and amplifies air temperatures (Pendergrass *et al* 2020, their figure 3). Therefore, soil moisture exerts opposing effects on air temperatures in these two regimes. Recent studies have highlighted significant drying and increased concurrent heatwave-drought events over IEA, potentially shifting toward water-limited conditions during hot extremes and intensifying hot-extreme warming (Zhang *et al* 2020b, Seo and Ha 2022). Using a soil moisture–temperature coupling strength index, Zhang *et al* (2020b, their figure 5) shows that positive soil moisture–temperature feedback existed over IEA, which had significantly intensified in recent decades. However, the relative importance of these physical processes in the EHEW over IEA, as well as their related drivers, remains incompletely understood.

In this article, we define the EHEW as the difference between the warming rates of daily maximum surface air temperature in hot days (TX90p) and summer-mean daily maximum surface air temperature (Tmax) from 1971 to 1990 (P1) to 2001–2020 (P2). To build a process-based understanding of this EHEW, we compute the 12 d air-parcel backward trajectories initiated on hot days across all IEA grids, and classify them up to six trajectories to reveal the potential contributions of the changes in heat-prone weather regimes to the EHEW. We then quantify the contributions of horizontal temperature advection, adiabatic warming, and diabatic heating to the EHEW using a Lagrangian temperature-anomaly equation along trajectories, further investigating the role of soil moisture deficiency over IEA and the surrounding regions.

2. Data and methods

2.1. Data

The 12 d backward trajectories are estimated using the horizontal winds and vertical velocity at model levels from the ERA5 data at a 3-hourly temporal resolution and a horizontal resolution of $0.5^\circ \times 0.5^\circ$ (Hersbach *et al* 2020). Additionally, 3-hourly temperatures on 137 model levels and radiation fluxes, as well as latent and sensible heat fluxes at the surface, are analyzed to investigate the physical processes along these trajectories. Daily Tmax, soil moisture, horizontal winds, and geopotential height at pressure levels are also derived from ERA5 for a comprehensive analysis.

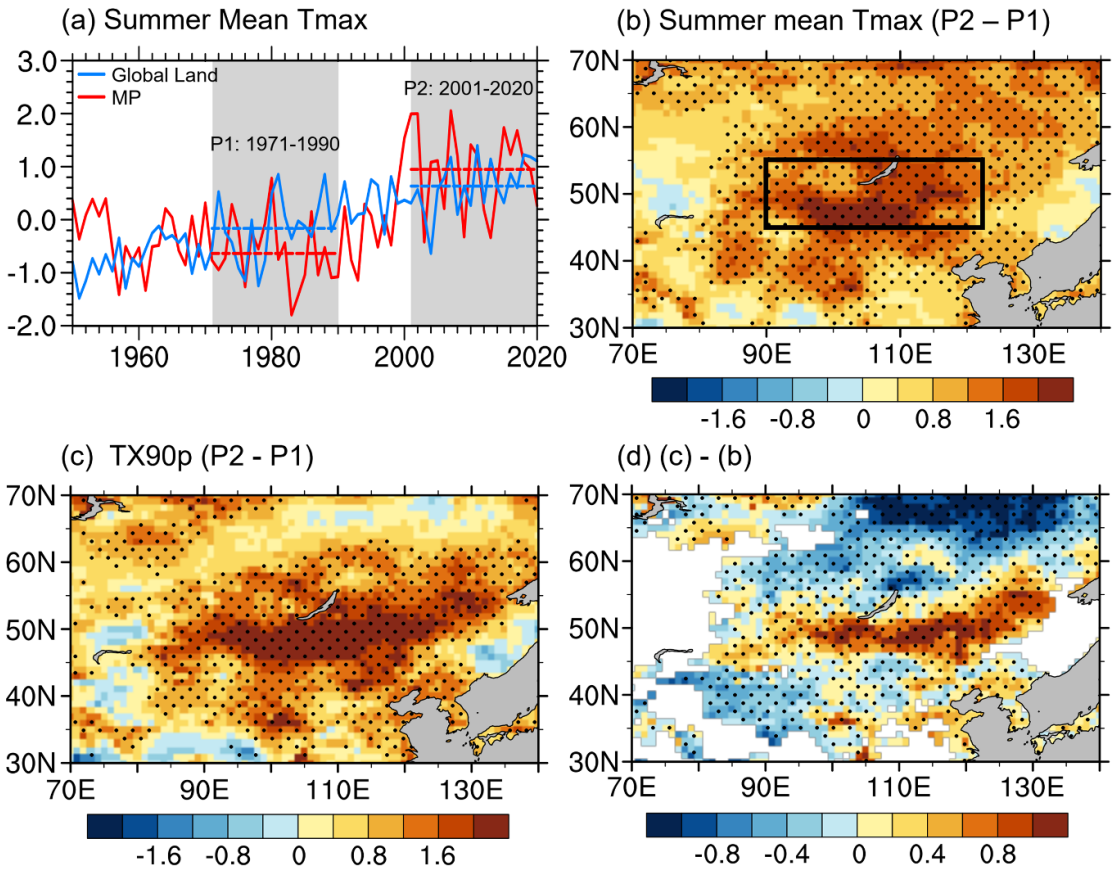

Figure 1. (a) Time series of summer (June-July-August) mean daily maximum surface air temperature (Tmax; °C) anomalies relative to the climatology of 1950–2020 over inner East Asia (IEA; red solid line) and global land (blue solid line). The dashed red and blue lines are the climatology of summer Tmax during 1971–1990 (P1) and 2001–2020 (P2) over IEA and global land, respectively. The gray shading highlights the two periods. Spatial patterns of the differences in (b) summer Tmax and (c) daily maximum surface air temperature in hot days (TX90p) between 2001–2020 and 1971–1990, and (d) their differences (excess hot-extreme warming). Black dots indicate the values that are statistically significant at the 0.05 level according to the student's *t*-test. The black rectangle in (b) represent IEA (45° –55° N, 90° –125° E).

2.2. Methods

Our analysis area IEA is referred to the region within 45° –55° N, 90° –125° E (figure 1(b)). It has been identified as a region where warming in this century may be beyond the tipping point (Zhang *et al* 2020b). Hot days are defined as the days when the daily Tmax exceeds the relative threshold, which is calculated as the daily 90th percentile of Tmax based on 15 d samples centered on each calendar day for the two distinct periods of 1971–1990 and 2001–2020, respectively. The temperature in hot days is named as TX90p (Fischer and Schaer 2010, Donat *et al* 2013). Summer is defined as June, July, and August.

To quantify the contributions of horizontal temperature advection, adiabatic warming, and diabatic heating to the near-surface extreme heat on hot days, we employ the Lagrangian temperature-anomaly equation along 12 days of backward trajectories, which is derived from the thermodynamic energy equation (Röthlisberger and Papritz 2023). These trajectories, estimated using LAGRANTO 2 (Sprenger and Wernli 2015), start from 10, 30, and 50 hPa above ground level at 09:00 UTC (the time of daily Tmax) during each hot day at all grid points over IEA, recorded at a 3-hourly temporal resolution. This approach results in a substantial dataset of approximately 1.3 million trajectories.

$$T'(x,t_h) = -\int_{t_g}^{t_h} \frac{\partial \overline{T}}{\partial t} \mathrm{d}\tau - \int_{t_g}^{t_h} v\nabla_h \overline{T} \mathrm{d}\tau + \int_{t_g}^{t_h} \left[\frac{\kappa T}{p} - \frac{\partial \overline{T}}{\partial p}\right] \times \omega \mathrm{d}\tau + \int_{t_g}^{t_h} \left(\frac{p}{p_0}\right)^{\kappa} \frac{\mathrm{D}\theta}{\mathrm{D}t} \mathrm{d}\tau. \quad (1)$$

For each hot day within the two periods, T' is the TX90p anomaly, which is the deviation of the model-level temperature T from the climatological $\overline{T}$. Here, $\overline{T}$ is computed separately for both periods by averaging over all calendar time steps on 15 day samples centered on that hot day. x denotes the position vector in three-dimensional geographical coordinates, v horizontal wind, ω vertical velocity, t time, p pressure, θ potential temperature, ∇_h horizontal gradient, κ dry adiabatic constant (0.286), and $p_0 = 1000$ hPa. $\int_{t_g}^{t_h} \mathrm{d}\tau$ is integrated along the backward trajectory from the last time when the temperature anomaly along the trajectory is zero (t_g) to the hot day (t_h),

reflecting the processes shaping T' (Röthlisberger and Papritz 2023, their extended data figure 7(a)). The terms on the right-hand side of equation (1) are referred to as seasonality T', advective T', adiabatic T' and diabatic T'. Seasonality T' arises from changes in the temperature climatology, including the daily cycle and seasonality, and is typically small. Advective T' results from the horizontal advection of the air parcel across climatological temperature gradients between t_g and t_h. Adiabatic T' creates temperature anomalies through adiabatic heating, and may be counteracted by vertical advection of climatological temperature subsidence. Diabatic T' arises from diabatic processes along the trajectory, including surface sensible heat flux and latent heat flux. Similarly, equation (1) can be integrated between arbitrary time steps to quantify the contribution of these processes to the evolution of temperature anomalies. Based on equation (1), the contributions of the physical processes leading to the change in TX90p anomalies can be quantified as follows:

$$\delta T' = \overline{T'}^{P2} - \overline{T'}^{P1} \tag{2}$$

where overbar denotes the average over 1971–1990 and 2001–2020, respectively. δ represents the change from 1971–1990 to 2001–2020. We will demonstrate that the change in TX90p anomalies is nearly identical to the EHEW.

To clearly illustrate the extensive trajectories and the evolution of temperature anomalies, we apply a curve clustering algorithm developed by Gaffney *et al* (2007). The algorithm considers the geographic locations and pressure levels along the trajectories, utilizing a finite mixture model where the data distribution is a convex linear combination of component density functions. The clustering process involves training a 4th order polynomial regression model for each trajectory, characterized by different shape parameters. Each trajectory is then assigned to a mixture component (or cluster) with the highest probability of generating it, based on the learned model parameters. This method has been widely employed in grouping tracks of tropical cyclones, atmospheric rivers, and moisture channels (Mei and Xie 2016, Cheng *et al* 2021, Huang *et al* 2022, Li *et al* 2023). The Matlab code for this algorithm is publicly available at www.datalab.uci.edu/software/CCT/.

After clustering the trajectories, the change in TX90p anomalies from 1971–1990 to 2001–2020 can be expressed as follows (Horton *et al* 2015):

$$\delta T' = \sum_{l=1}^{K} \delta\left(\overline{T'_l} * \overline{f_l}\right) = \sum_{l=1}^{K} \left\{ \delta\overline{T'_l} * \overline{f_l}^{P1} + \overline{T'_l}^{P1} * \delta\overline{f_l} + \delta\overline{T'_l} * \delta\overline{f_l} \right\} \tag{3}$$

in which K represents the total number of clustered trajectory and f_l denotes the frequency of clustered trajectory l. K is set to be 6 based on the small and fluctuating gradients of the trained log-likelihood (figure S1(b)), which effectively characterizes the trajectory types and their links to large-scale circulations. Thus, the change in TX90p anomalies can be decomposed into the terms on the right-hand side of equation (3). Specifically, it arises from the changes in TX90p anomalies for each clustered trajectory, which may be driven by the changes in the temperature evolution of air parcels along trajectories, the changes in the frequency of clustered trajectories associated with variations in heat-prone weather regimes and the interaction between these changes. A similar method can be applied to other variables to quantify the relative impact of evaporative fraction (EF) and total surface heat flux on the changes in sensible heat flux:

$$\mathrm{EF} = \frac{Q_e}{Q_e + Q_h} = \frac{Q_e}{Q_s} \tag{4}$$

$$\delta Q_h = \delta Q_s * \left(1 - \overline{\mathrm{EF}}^{P1}\right) + \overline{Q_s}^{P1} * (1 - \delta\mathrm{EF}) + \delta Q_s (1 - \delta\mathrm{EF}) \tag{5}$$

where EF is the EF, and the total surface heat flux Q_s is the sum of latent heat flux Q_e and sensible heat flux Q_h.

3. Result

3.1. Excess warming of extremely hot temperature compared to the summer mean in recent decades

The summer mean Tmax anomalies averaged over IEA exhibit an abrupt warming in recent decades, featuring a remarkable warming during 2001–2020 compared to 1971–1990 (figure 1(a); 1.6 °C), with the most pronounced increase in southern IEA (figure 1(b)). This abrupt warming in IEA is notably larger than that in the surrounding regions, being twice the global land average (figure 1(a)), and more than three times the global land average in southern IEA (figure 1(b)). Moreover, TX90p has warmed more rapidly than the summer mean Tmax, with an excess warming of about 0.5 °C over IEA (figure 1(d)). In southern IEA, the warming of TX90p is nearly twice that of summer mean Tmax (figure 1(d)). Consequently, IEA emerges as a hotspot, experiencing faster warming of TX90p than the summer mean Tmax (the EHEW) during 2001–2020 relative to 1971–1990, and aligning with the finding from previous studies (Wang *et al* 2022).

3.2. Limited impacts of the changes in corridor frequency on the EHEW during recent decades

As revealed in figure S1(a), the change in TX90p anomalies defined in equation (1) is nearly identical to the EHEW (figure 1(d)). To understand the physical processes driving the evolution of temperature in generating TX90p anomalies over IEA, we estimate 12 d backward trajectories for the air parcels originating near the surface during hot days in 1971–1990 and

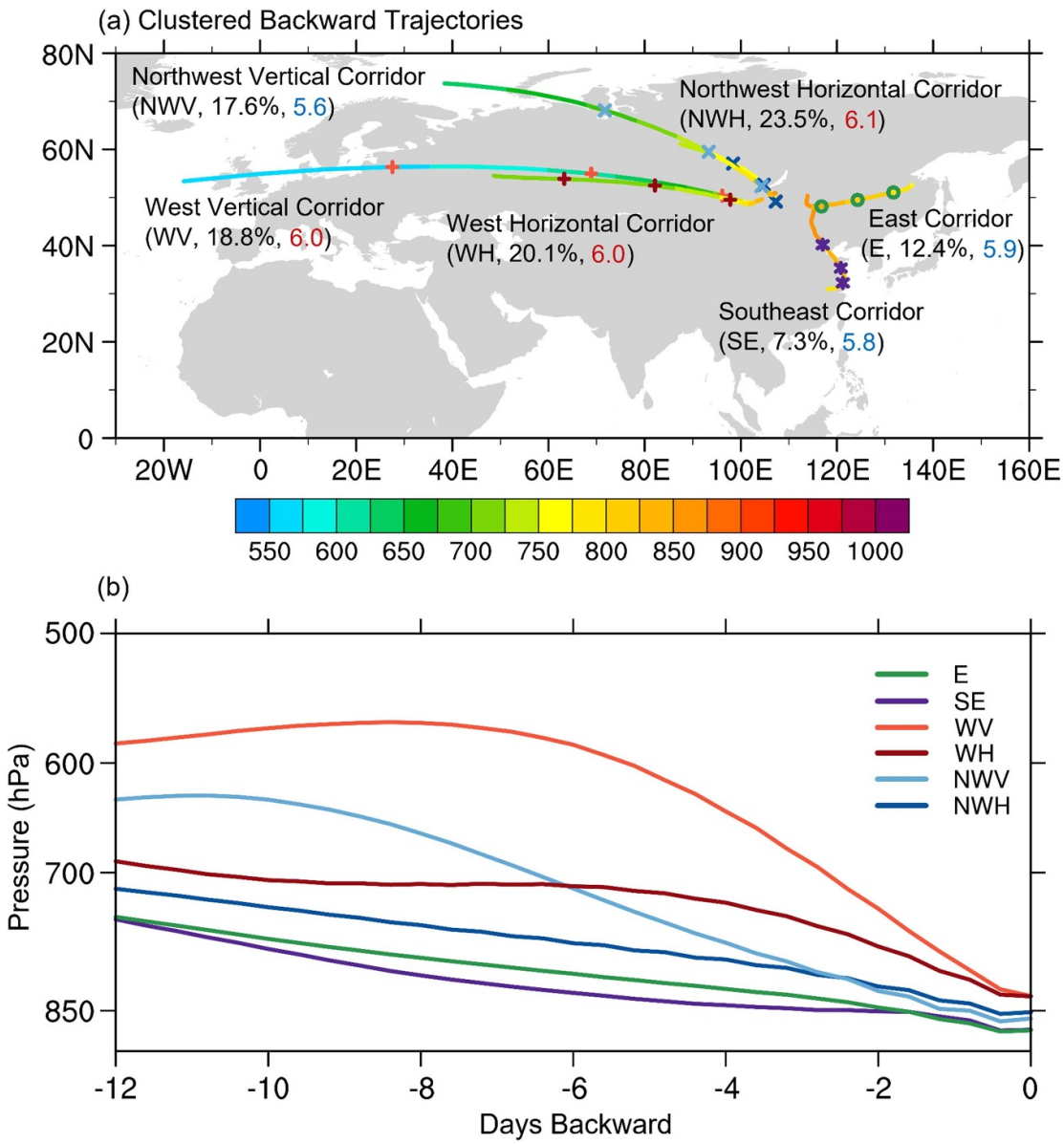

Figure 2. (a) Cluster mean regression curves of the 12 d backward trajectories initiated at near-surface levels on hot days during 1971–1990 and 2001–2020, shaded by the cluster mean pressure (hPa). Marks along curves indicate positions at days −3, −6, and −9. The black numbers in brackets are the corridor frequencies during 1971–1990 and 2001–2020. The red (blue) numbers indicate that the composite TX90p anomalies for the corridors are warmer (colder) than those for all hot days. (b) Temporal evolution of pressure along each corridor. The *x*-axis represents the time (day) from the hot days.

2001–2020. The influence of physical processes on the temperature evolution along these trajectories is assessed using the Lagrangian temperature-anomaly equation (equation (1)).

Six clustered trajectories are selected and named: northwest horizontal, northwest vertical, west horizontal, west vertical, southeast, and east corridors (figure 2(a)). Air parcels descending along these corridors approach IEA and lead to TX90p (figures 2(b) and S9). Relative to 1971–1990, the frequency of the east corridor has increased remarkably during 2001–2020, with a slight increase in both horizontal corridors (black bars in figure 3(b)).

To reveal how circulation changes may lead to these frequency changes, we identify the critical patterns that favor each corridor through a composite analysis of time-evolving circulation based on selected days. These days are chosen when both the daily number and percentage of trajectories in the corridor exceed the 90th percentile of all days with at least one grid experiencing a hot day during 1971–1990 and 2001–2020 (more than 28 d for each corridor). In general, the critical patterns for different corridors associated with the hot-extreme temperatures over IEA are characterized by synoptic-scale waves, with a significant local anticyclone anomaly or ridge when

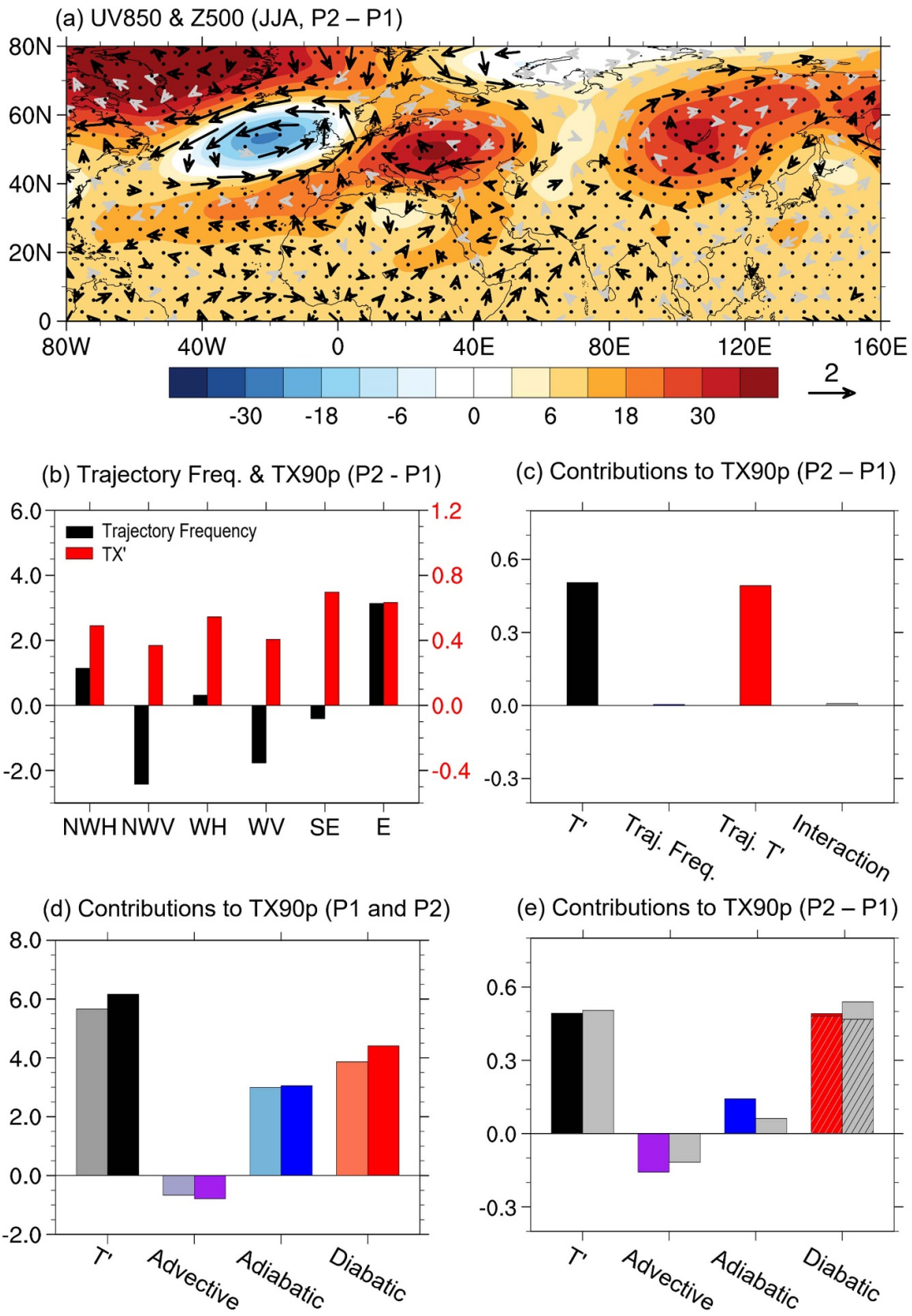

Figure 3. (a) Spatial patterns of differences in horizontal wind (m s^{-1}, vectors) at 850 hPa and geopotential height (gpm, shading) at 500 hPa in summer between 2001–2020 and 1971–1990. Black dots mark the values exceeding the 0.05 significance level for changes in height. (b) Changes in TX90p anomalies (red) and frequency (black) of each corridor. (c) Changes in TX90p anomalies (nearly identical to the EHEW), along with contributions from changes in corridor frequency, shifts in corridor TX90p anomalies, and their interactions. (d) TX90p anomalies, its components induced by advective process, adiabatic heating, and diabatic heating during 1971–1990 (lighter color bars) and 2001–2020 (darker color bars), as well as (e) their differences. Hatched bar is diabatic heating along trajectories averaged from day −2 to day 0. Colored bars and gray bars in (e) represent the results without and with the impacts of change in the corridor frequencies, respectively.

hot-extreme occurs ($t = 0$). However, these waves exhibit varying amplitudes, propagation trajectories, wave numbers, and phase speeds (figures S2–S7).

The vertical and horizontal corridors associated with a similar wave train propagates towards IEA (figures S2 vs. S3 and S4 vs. S5). Among these, the horizontal corridors are linked to more intense wave trains, characterized by prolonged and strongly eastward-propagating ridges over IEA, where diabatic heating plays a more important role in warming the parcels (figures S8(a) vs. S8(b) and S8(c) vs. S8(d)). These prolonged and strong ridges benefit the horizontal corridors by persistently heating the low-level air, thereby shaping TX90p with weaker adiabatic heating.

In the east corridor, air parcels descend along the westerlies on the south side of a strong and persistent anticyclone anomaly over northeast Asia, primarily heated by diabatic processes (figures S7 and S8(f)). These westerlies, shaped by the strong anticyclone and the anomalous low pressure southeast of the anticyclone, may be part of a persistent wavenumber-4 pattern.

The increased frequencies for horizontal and eastern corridors from 1971–1990 to 2001–2020 may be linked to summer circulation changes over Eurasia, characterized by an atmospheric wave train featuring an anticyclonic anomaly over IEA, potentially strengthening and prolonging the synoptic-scale anticyclonic pattern *in situ* (figure 3(a)). These circulation changes could be induced by the phase changes in both the IPV and the AMV over recent decades, as evidenced by both observational data and model simulations (Piao *et al* 2017, Zhang *et al* 2020a, Sun *et al* 2022, Cai *et al* 2024, Zhang *et al* 2024b). Land–atmosphere coupling can further intensify the anticyclonic anomaly over IEA by warming the land surface through increased shortwave radiation related to reduced cloud cover (Zhang *et al* 2020b). This warming subsequently heats the overlying atmosphere due to increased upward long-wave radiation and sensible heat flux, thereby reinforcing the anticyclone. Moreover, Yang *et al* (2024) noted a phase-locking behavior of an amplified wavenumber-4 pattern with an anomalous ridge over IEA since the mid-1990s, which has also contributed to the increased frequency of the east corridor.

By linearizing equation (3), we quantify how the increase in TX90p anomalies for each corridor (red bars in figure 3(b)) and the changes in corridor frequencies affect the EHEW from 1971–1990 to 2001–2020. The results demonstrate that the EHEW is primarily induced by the consistent increase in TX90p anomalies in the recent decades (red bar in figure 3(c)). The changes in the corridor frequency, associated with the change in heat-prone weather regimes over Eurasia, exert only a limited influence on the EHEW (figure 3(c)).

3.3. Impacts of soil drying on the EHEW in recent decades

To better comprehend the possible mechanisms for the EHEW, we use equations (1) and (2) to quantitatively estimate the related physical processes. For both 1971–1990 and 2001–2020, TX90p anomalies are induced by both adiabatic heating and diabatic heating, while the advective process has a weak cooling effect (figure 3(d)). However, the EHEW from 1971–1990 to 2001–2020 is predominantly driven by enhanced diabatic heating (figure 3(e)), while the changes in synoptic-scale circulation regimes appear to have a limited influence (color vs. gray bars in figure 3(e)). Notably, approximately 88.6% of the enhanced diabatic heating occurs from day −2 to day 0 (hatched bar in figure 3(e)), with the vast majority of air partials already situated within IEA at day −2 (figure S9(a)), suggesting that the enhanced diabatic heating is dominated by localized processes over IEA.

We further propose a potential driver for this locally enhanced diabatic heating from 1971–1990 to 2001–2020. IEA has experienced a significant reduction in the summer soil moisture (figure 4(a)), consistent with the findings of Zhang *et al* (2020b) from both observations and reanalysis datasets (their figure 2). This summer soil drying leads to hot days under drier conditions, especially in southern IEA (figure 4(b)). As discussed in section 1 and revealed by the reduced EF along trajectories from day −2 to day 0 in recent decades (figure 4(c)), this drier condition could shift soil moisture–temperature interaction into a water-limited regime. This result is further supported by the positive (negative) relationship between soil moisture and latent heat flux over IEA on dry (wet) days (figure S9), with dry days defined as the days with soil moisture below −2 standard deviations and wet days above 2 standard deviations. The drier conditions on hot days may benefit the soil moisture–temperature feedback under water-limited conditions, where limited soil moisture reduces latent heat flux and enhances sensible heat flux by altering surface energy partitioning, leading to EHEW. According to the linearized equation (5), about 71.2% of the increased sensible heat fluxes averaged within 2 days before the hot days are contributed by the reduced EF, with a much smaller contribution from the increased net surface radiation flux (29.2%, figure 4(d)). Moreover, soil moisture depletion can reduce cloud cover, allowing the land surface to receive more solar shortwave radiation, thus increasing sensible heat flux. Furthermore, the changes in soil moisture during hot days closely align with the spatial patterns of the EHEW across IEA and its surroundings (figures 1(d) and 4(b)), with a significant spatial correlation coefficient of −0.66, underscoring the critical role of soil drying and reduced EF in driving the EHEW during recent decades.

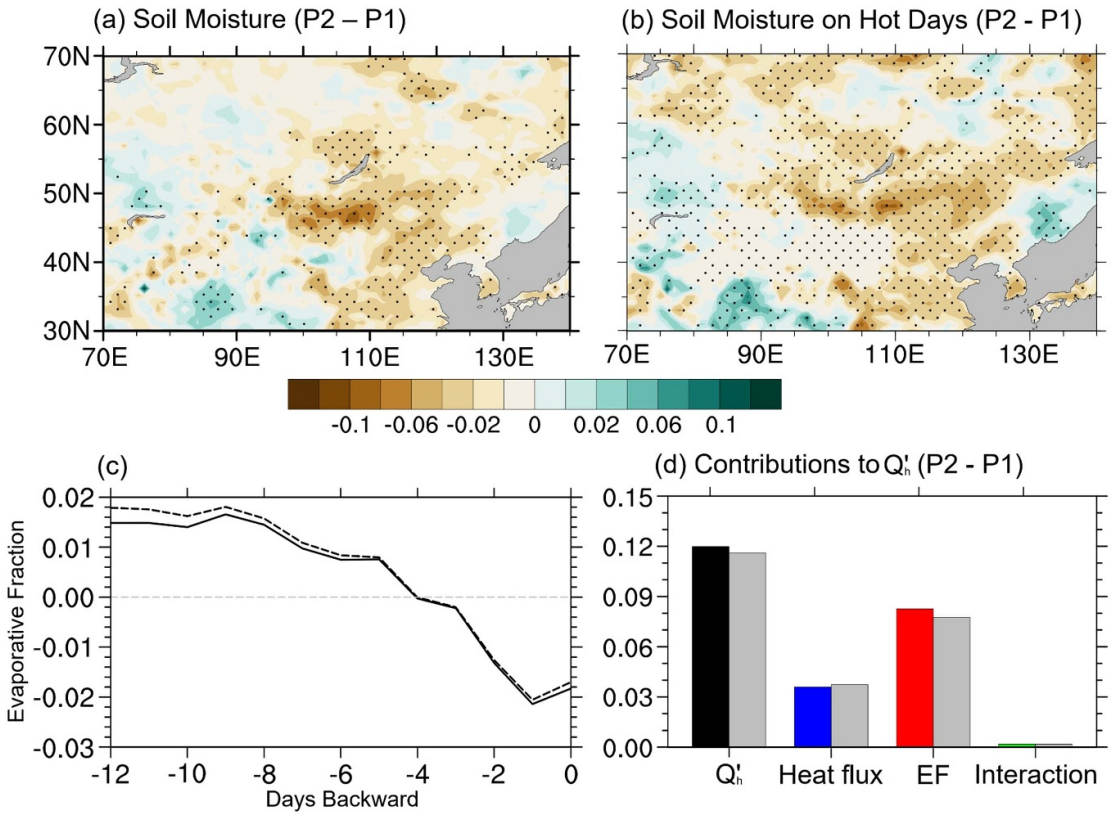

Figure 4. (a) Spatial patterns of differences in summer soil moisture (m^3 m^{-3}) between 2001–2020 and 1971–1990. (b) Changes in soil moisture during hot days between 2001–2020 and 1971–1990. (c) Temporal evolution of shifts in evaporative fraction along trajectories. The solid and dashed lines represent the results without and with the impacts of changes in corridor frequencies, respectively. (d) Changes in sensible heat flux along trajectories averaged from day −2 to day 0, with contributions from shifts in total surface heat flux (10^{-5} W m^{-2}), changes in evaporative fraction, and their interactions. Colored bars represent results without the impact of corridor frequency changes, while the gray bars include this impact.

4. Summary and discussion

Relative to 1971–1990, IEA has experienced a remarkable excess warming of TX90p compared to the summer mean Tmax during 2001–2020. This EHEW is more pronounced over southern IEA and is 2 times the summer Tmax change, making ecosystems more vulnerable to climate change and human activities. Utilizing a Lagrangian temperature-anomaly equation along an air-parcel trajectory, we find that the EHEW is predominantly due to increased diabatic heating, most of which occurs within 2 days before the hot days and is likely to be related to enhanced sensible heat flux. About 71.2% of the increased sensible heat flux is induced by the changes in surface energy partitioning along trajectories from 1971–1990 to 2001–2020, which could be driven by soil drying over IEA. Additionally, curve clustering results show that the changes in the frequency of clustered trajectories have a limited impact on the EHEW, indicating a small contribution from the changes in synoptic-scale circulation regimes. Similar results in this paper can be mainly achieved with 10 d or 14 d backward trajectories.

Our quantitative results emphasize the critical role of soil drying in leading to EHEW over IEA. Soil drying may arise from anticyclonic circulation changes over IEA, which may reduce precipitation and enhance the positive soil moisture–temperature feedback (Piao *et al* 2017, Zhang *et al* 2020b). These circulation changes may be induced by the phase shifts in the AMV and the IPV (Cai *et al* 2024). In addition to natural drivers, increased anthropogenic greenhouse gas emissions and decreased anthropogenic aerosols over North America and Europe since the mid-1970s have been reported as the main drivers of warming over IEA (Sprenger and Wernli 2015, Dong *et al* 2016, Zhou *et al* 2020, Hua *et al* 2021, Zhang *et al* 2024b), which could trigger positive soil moisture–temperature feedback. As temperatures rise, the atmospheric vapor pressure deficit increases, leading to soil drying and further enhancing the initial temperature increase (Seneviratne *et al* 2010, Seo and Ha 2022). Moreover, overgrazing could exacerbate soil drying by contributing to widespread grassland decline (Nandintsetseg *et al* 2021, Zhang *et al* 2024a, Cai *et al* 2024).

The contributions of various drivers of this drying require further quantitative investigations, including the roles of natural internal variability, human-induced greenhouse gases, aerosol

emissions, water withdrawals, and overgrazing. Additionally, accurately simulating soil drying and related land-atmosphere feedback is crucial for future projections of extreme heat changes and could help constrain hot-extreme projections in climate models. In the future, the EHEW may be amplified as global warming could continue to dry soils and shift land-atmosphere interactions into water-limited conditions (Qiao *et al* 2023). Policymakers should take action to sustain soil moisture, such as maintaining ecosystem stability and controlling livestock numbers, to mitigate the risk of severe heatwaves, droughts, serious economic losses, and threats to food security.

Data availability statement

The data that support the findings of this study are openly available at the following URL/DOI: https://climate.copernicus.eu/climate-reanalysis.

Acknowledgment

The authors are grateful to all data providers. This research was supported by the Innovation Group Project of the Southern Marine Science and Engineering Guangdong Laboratory (Zhuhai) (316323005), the National Natural Science Foundation of China (42375029), the Guangdong Basic and Applied Basic Research Foundation (2023A1515010908), the Guangdong Province Key Laboratory for Climate Change and Natural Disaster Studies (2023B1212060019), and the International Program for PhD Candidates (Sun Yat-sen University). BD was supported by the UK National Centre for Atmospheric Science, funded by the Natural Environment Research Council (NERC) and his contribution was also supported by the Towards an Integrated Capability to Explain and Predict Regional Climate Changes (EXPECT) project by the European Union's Horizon Europe research and innovation programme under Grant Agreement No. 101137656. The authors would like to thank the two anonymous reviewers for their valuable comments and suggestions on an early version of the paper.

Conflict of interest

The authors declare no conflicts of interest or competing interests.

ORCID iDs

Zejiang Yin https://orcid.org/0009-0005-8542-6258
Buwen Dong https://orcid.org/0000-0003-0809-7911
Song Yang https://orcid.org/0000-0003-1840-8429
Wei Wei https://orcid.org/0000-0002-7620-8954

References

Bouwman A F, Van der Hoek K W, Eickhout B and Soenario I 2005 Exploring changes in world ruminant production systems *Agric. Syst.* **84** 121–53
Cai F, Liu C, Gerten D, Yang S, Zhang T, Lin S and Kurths J 2024 Pronounced spatial disparity of projected heatwave changes linked to heat domes and land-atmosphere coupling *npj Clim. Atmos. Sci.* **7**
Cai Q, Chen W, Chen S, Xie SP, Piao J, Ma T and Lan X 2024 Recent pronounced warming on the Mongolian Plateau boosted by internal climate variability *Nat. Geosci.* **17** 181–8
Cai W *et al* 2019 Pantropical climate interactions *Science* **363** eaav4236
Chen Q, Timmermans J, Wen W and van Bodegom P M 2023 Ecosystems threatened by intensified drought with divergent vulnerability *Remote Sens. Environ.* **289** 113512
Cheng T F, Lu M and Dai L 2021 Moisture channels and pre-existing weather systems for East Asian rain belts *npj Clim. Atmos. Sci.* **4** 32
Donat M G *et al* 2013 Updated analyses of temperature and precipitation extreme indices since the beginning of the twentieth century: the HadEX2 dataset *J. Geophys. Res. Atmos.* **118** 2098–118
Donat M G and Alexander L V 2012 The shifting probability distribution of global daytime and night-time temperatures *Geophys. Res. Lett.* **39** L14707
Dong B, Sutton R T, Chen W, Liu X, Lu R and Sun Y 2016 Abrupt summer warming and changes in temperature extremes over Northeast Asia since the mid-1990s: drivers and physical processes *Adv. Atmos. Sci.* **33** 1005–23
Easterling D R, Meehl G A, Parmesan C, Changnon S A, Karl T R and Mearns L O 2000 Climate extremes: observations, modeling, and impacts *Science* **289** 2068–74
Fischer E M and Schär C 2010 Consistent geographical patterns of changes in high-impact European heatwaves *Nat. Geosci.* **3** 398–403
Gaffney S J, Robertson A W, Smyth P, Camargo S J and Ghil M 2007 Probabilistic clustering of extratropical cyclones using regression mixture models *Clim. Dyn.* **29** 423–40
Gang C, Zhou W, Chen Y, Wang Z, Sun Z, Li J, Qi J and Odeh I 2014 Quantitative assessment of the contributions of climate change and human activities on global grassland degradation *Environ. Earth Sci.* **72** 4273–82
Hersbach H *et al* 2020 The ERA5 global reanalysis Q. *J. R. Meteorol. Soc.* **146** 1999–2049
Hilker T, Natsagdorj E, Waring R H, Lyapustin A and Wang Y 2014 Satellite observed widespread decline in Mongolian grasslands largely due to overgrazing *Glob. Change Biol.* **20** 418–28
Hong X, Lu R and Li S 2017 Amplified summer warming in Europe–West Asia and Northeast Asia after the mid-1990s *Environ. Res. Lett.* **12** 094007
Horton D E, Johnson N C, Singh D, Swain D L, Rajaratnam B and Diffenbaugh N S 2015 Contribution of changes in atmospheric circulation patterns to extreme temperature trends *Nature* **522** 465–9
Hua W, Qin M, Dai A, Zhou L, Chen H and Zhang W 2021 Reconciling human and natural drivers of the tripole pattern of multidecadal summer temperature variations over Eurasia *Geophys. Res. Lett.* **48** e2021GL093971
Huang C, Liu H, Wang X, Li H, Zhang Z, Zuo J and Wang R 2022 PDO modulation on the relationship between ENSO and typhoon tracks *J. Clim.* **35** 6703–20
Kornhuber K, Osprey S, Coumou D, Petri S, Petoukhov V, Rahmstorf S and Gray L 2019 Extreme weather events in early summer 2018 connected by a recurrent hemispheric wave-7 pattern *Environ. Res. Lett.* **14** 054002

Lewis S C and King A D 2017 Evolution of mean, variance and extremes in 21st century temperatures *Weather Clim. Extremes* **15** 1–10

Li C, Mei W and Kamae Y 2023 A cluster analysis of cold-season atmospheric river tracks over the North Atlantic and their linkages to extreme precipitation and winds *Clim. Dyn.* **60** 201–12

Mann M E, Rahmstorf S, Kornhuber K, Steinman B A, Miller S K and Coumou D 2017 Influence of anthropogenic climate change on planetary wave resonance and extreme weather events *Sci. Rep.* **7** 45242

Mei W and Xie SP 2016 Intensification of landfalling typhoons over the northwest Pacific since the late 1970s *Nat. Geosci.* **9** 753–7

Na L, Na R, Bao Y and Zhang J 2021 Time-lagged correlation between soil moisture and intra-annual dynamics of vegetation on the Mongolian Plateau *Remote Sens.* **13** 1527

Nandintsetseg B, Boldgiv B, Chang J, Ciais P, Davaanyam E, Batbold A, Bat-Oyun T and Stenseth N C 2021 Risk and vulnerability of Mongolian grasslands under climate change *Environ. Res. Lett.* **16** 034035

Patterson M 2023 North-West Europe hottest days are warming twice as fast as mean summer days *Geophys. Res. Lett.* **50** e2023GL102757

Pendergrass A G *et al* 2020 Flash droughts present a new challenge for subseasonal-to-seasonal prediction *Nat. Clim. Change* **10** 191–9

Perkins S E, Argüeso D and White C J 2015 Relationships between climate variability, soil moisture, and Australian heatwaves *J. Geophys. Res. Atmos.* **120** 8144–64

Piao J, Chen W, Wei K, Liu Y, Graf HF, Ahn JB and Pogoreltsev A 2017 An abrupt rainfall decrease over the Asian inland plateau region around 1999 and the possible underlying mechanism *Adv. Atmos. Sci.* **34** 456–68

Qiao L, Zuo Z, Zhang R, Piao S, Xiao D and Zhang K 2023 Soil moisture–atmosphere coupling accelerates global warming *Nat. Commun.* **14** 4908

Röthlisberger M and Papritz L 2023 Quantifying the physical processes leading to atmospheric hot extremes at a global scale *Nat. Geosci.* **16** 210–6

Seneviratne S I, Corti T, Davin E L, Hirschi M, Jaeger E B, Lehner I, Orlowsky B and Teuling A J 2010 Investigating soil moisture–climate interactions in a changing climate: a review *Earth-Sci. Rev.* **99** 125–61

Seneviratne S I, Lüthi D, Litschi M and Schär C 2006 Land–atmosphere coupling and climate change in Europe *Nature* **443** 205–9

Seo YW and Ha KJ 2022 Changes in land-atmosphere coupling increase compound drought and heatwaves over northern East Asia *npj Clim. Atmos. Sci.* **5** 100

Sprenger M and Wernli H 2015 The LAGRANTO Lagrangian analysis tool – version 2.0 *Geosci. Model Dev.* **8** 2569–86

Sun X, Ding Q, Wang SY S, Topál D, Li Q, Castro C, Teng H, Luo R and Ding Y 2022 Enhanced jet stream waviness induced by suppressed tropical Pacific convection during boreal summer *Nat. Commun.* **13** 1288

Tamarin-Brodsky T, Hodges K, Hoskins B J and Shepherd T G 2022 A simple model for interpreting temperature variability and its higher-order changes *J. Clim.* **35** 387–403

Teng H and Branstator G 2019 Amplification of waveguide teleconnections in the boreal summer *Curr. Clim. Change Rep.* **5** 421–32

Wang R, Gentine P, Li L, Chen J, Ning L, Yuan L and Lü G 2022 Observational evidence of regional increasing hot extreme accelerated by surface energy partitioning *J. Hydrometeorol.* **23** 491–501

Yang X, Zeng G, Zhang S, Iyakaremye V, Shen C, Wang WC and Chen D 2024 Phase-locked Rossby wave-4 pattern dominates the 2022-like concurrent heat extremes across the Northern Hemisphere *Geophys. Res. Lett.* **51** e2023GL107106

Zhang G *et al* 2024a Biodiversity and wetting of climate alleviate vegetation vulnerability under compound drought-hot extremes *Geophys. Res. Lett.* **51** e2024GL108396

Zhang G, Zeng G, Li C and Yang X 2020a Impact of PDO and AMO on interdecadal variability in extreme high temperatures in North China over the most recent 40-year period *Clim. Dyn.* **54** 3003–20

Zhang K, Zuo Z, Suarez-Gutierrez L and Bu L 2024b The significant influence of the Atlantic multidecadal variability to the abrupt warming in Northeast Asia in the 1990s *npj Clim. Atmos. Sci.* **7** 28

Zhang P, Jeong JH, Yoon JH, Kim H, Wang SY S, Linderholm H W, Fang K, Wu X and Chen D 2020b Abrupt shift to hotter and drier climate over inner East Asia beyond the tipping point *Science* **370** 1095–9

Zhang Y, Wang Q, Wang Z, Yang Y and Li J 2020c Impact of human activities and climate change on the grassland dynamics under different regime policies in the Mongolian Plateau *Sci. Total Environ.* **698** 134304

Zhao X, Shen H, Geng X and Fang J 2021 Three-decadal destabilization of vegetation activity on the Mongolian Plateau *Environ. Res. Lett.* **16** 034049

Zhou C Y, Qiao L, Zhang R, Chen D, Piao S, Xiao D and Zhang K 2020 An interdecadal change of summer atmospheric circulation over Asian mid-high latitudes and associated effects *J. Tropical Meteorol.* **26** 363–76

Zuo Z, Qiao L, Zhang R, Chen D, Piao S, Xiao D and Zhang K 2024 Importance of soil moisture conservation in mitigating climate change *Sci. Bull.* **69** 1332–41